encit 2020

ABCM Associação Brasileira de Engenharia e Ciências Mecânicas

18th Brazilian Congress of Thermal Sciences and Engineering
November 16–20, 2020 (Online)

ENC-2020-0169
DETERMINING THE SERVICE AND ABSOLUTE CEILINGS OF BATTERY-POWERED ELECTRIC AIRCRAFT

Guilherme N. Barufaldi
Roberto Gil A. da Silva
Instituto Tecnológico de Aeronáutica, Praça Mal. Eduardo Gomes, 50, Vila das Acácias, CEP: 12228-900, São José dos Campos – SP – Brazil
guilherme.barufaldi@protonmail.com, gil@ita.br

Abstract.
Electric propulsion for airplanes is becoming a reality. This aviation market segment has grown considerably during the last decades and, in the next years, light general aviation and training airplanes are expected to become operational. Due to many factors, batteries are still the main power source currently in use for electric propulsion. Recent studies have shown the performance potential of battery-powered airplanes. Among the particular characteristics of these aircraft is the capacity to reach significantly higher altitudes than aircraft powered by internal combustion engines. This work presents a method for calculating the service and absolute ceilings of such type of aircraft, i.e., the maximum altitudes that can be reached. These quantities are important to determine suitable altitudes for cruise flight and other operational characteristics. The method is based on a combination of analytical and numerical computation procedures and take into account motor and propeller data. Aircraft, motor and battery models are presented in parametric form, together with the characteristic curves of a fixed pitch propeller. Numerical results are obtained and show that high altitudes may indeed be reached.

Keywords: *Electric aircraft, electric propulsion, flight performance, climb performance, green aircraft*

1. INTRODUCTION

Electric propulsion for airplanes is becoming a reality. From small unmanned aerial vehicles (UAVs) to manned light sporting aircraft and sailplanes, many vehicles are being equipped with this type of propulsion system. This aviation market segment has grown considerably during the last decades, since the Lange Antares 20E motor glider received its airworthiness certificate in 2003 – the first ever issued for an electric aircraft (Lange Aviation, 2003). In the next decade, light general aviation and training airplanes are expected to become operational (Moore and Fredericks, 2014), and even larger aircraft are currently being studied, such as the Airbus E-Fan X (Airbus Group, 2017).

An all-electric propulsion system usually consists of a propeller or ducted fan driven by an electric motor, which is powered by batteries, solar panels or fuel cells, or a combination of these devices. However, due to many factors, batteries are still the main power source currently in use for all-electric airplanes (Brelje and Martins, 2019). Although the relatively low energy density of batteries severely constrains the application of these devices on large commercial airplanes (Hepperle, 2012), the power output capacity of batteries is currently superior to that of fuel cells and solar panels. Moreover, batteries are significantly easier to handle and do not require constant refueling, making it the preferred choice to power electric airplanes.

Sachs (2013) showed that since the electric motor is not an air-breathing device, an all-electric airplane can reach significantly higher altitudes than airplanes equipped with internal combustion engines. As a consequence, this type of aircraft can achieve higher velocities. An important result of Sachs' formulation is that the velocity for maximum range could be equal to the maximum velocity, provided the aircraft is able to achieve the altitude at which this happens. Barufaldi *et al.* (2019) derived parametric analytical solutions for energy-optimal climb performance, obtaining steady climb trajectories that minimize the total electric energy spent. However, none of the previously mentioned works show ways to calculate the altitude limits electric airplanes may reach, nor do they take into account the characteristics of the propeller, at least not in an explicit fashion.

This work presents a method to determine the the service and absolute ceilings of electric aircraft powered by batteries, i.e., the maximum altitude values at which the aircraft can sustain flight. The calculation of these quantities is important to analyze not only the altitude capability of such aircraft, but also suitable and ideal altitudes for cruise flight, among other important operational characteristics. The method developed in this article is based on a combination of analytical and numerical computation procedures, and take into account motor and propeller characteristics. Parametric models of

the aircraft, battery and electric motor are provided, together with characteristic curves of an all-composite fixed pitch propeller. Numerical results are obtained to illustrate the method implementation and to show that high altitudes can be reached.

2. AIRCRAFT MODELING

2.1 Aerodynamics

The service ceiling is reached when the aircraft is no longer able to maintain a minimum rate of climb (ROC) of 100 ft/min, and the absolute ceiling is the altitude at which the aircraft is no longer able to climb at all. For this analysis, a regular climb with leveled wings is assumed, i.e., no lateral or directional movements occur. Since the climb angle γ is usually small (in radians) for propeller-driven aircraft, then $\cos\gamma \approx 1$ is a good approximation, and the equilibrium of external forces acting on the aircraft can be expressed by the following equations (Anderson, 1999):

$$T - D - W\sin\gamma = 0 \tag{1}$$

$$L = W \tag{2}$$

where W is the aircraft weight; T is the propeller thrust; γ is the flightpath (climb) angle; and L and D are the components of the aerodynamic force, known as lift and drag, respectively. L and D are calculated according to Eqs. (3) and (4), respectively:

$$L = \frac{\rho V^2}{2} S C_L \tag{3}$$

$$D = \frac{\rho V^2}{2} S C_D \tag{4}$$

where V is the aircraft velocity (true airspeed); ρ is the air density; S is the wing reference area; C_L is the dimensionless lift coefficient; and C_D is the dimensionless drag coefficient. Since electric airplanes fly at low subsonic airspeeds, compressibility effects can be neglected and C_D is modeled as a quadratic function of the lift coefficient only (Anderson, 2010):

$$C_D = C_{D_0} + k \cdot C_L^2 \tag{5}$$

where C_{D_0} is the zero lift drag coefficient, and k is the lift-dependent drag constant.

2.2 Propeller

The aircraft is assumed to be equipped with a fixed-pitch propeller, which is very common in small general aviation airplanes, due to its simplicity, lower cost and lighter weight (Raymer, 2006). The propeller thrust T and its aerodynamic torque Q_{pr} are given by the following equations:

$$T = \rho\, C_T\, n^2 d^4 \tag{6}$$

$$Q_{\text{pr}} = \rho\, C_Q\, n^2 d^5 \tag{7}$$

where C_T and C_Q are the propeller thrust and torque dimensionless coefficients, respectively; n is the propeller rotation frequency, in Hz (rotations per second); and d is the propeller diameter. For a given propeller, C_T and C_Q are usually provided in charts – known as the characteristic curves of that propeller –, as functions of a dimensionless parameter J known as advance ratio, defined according to Eq. (8) (Von Mises, 1945).

$$J = \frac{V}{n\, d} \tag{8}$$

2.3 Battery

Tremblay and Dessaint (2009) proposed a model for the battery voltage as a function of the state of charge (SOC). The model incorporates terms for the exponential zone, for the polarization resistance and also a linear term to account for the voltage dynamics when the current varies. For relatively short periods of time, no significant variation of the SOC occurs, and the open circuit voltage can be considered constant.

Since in this work only the instantaneous power is analyzed, the terms involving the SOC are neglected and the open circuit voltage U_0 is considered constant. A linear term is employed to account for the output voltage U_{out} variation caused by "ohmic" losses. Figure 1 depicts the battery lumped circuit model, with a constant internal resistance R_{bat}.

Equation (9) shows the output voltage U_{out} as a function of the electric current i.

$$U_{\text{out}} = U_0 - i \cdot R_{\text{bat}} \tag{9}$$

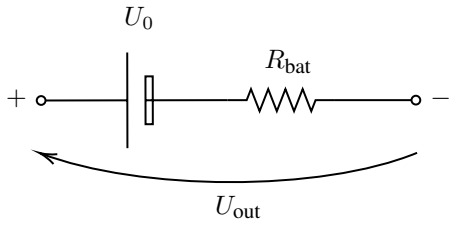

Figure 1. Linear lumped circuit model for the battery.

2.4 Electric motor

A high-level block diagram of the electric propulsion system is shown in Fig. 2. A brushless DC motor drives a shaft to which a propeller is connected. The controller regulates the rotation speed by sending pulses of electric current (PWM – pulse-width modulation) from the battery to the motor.

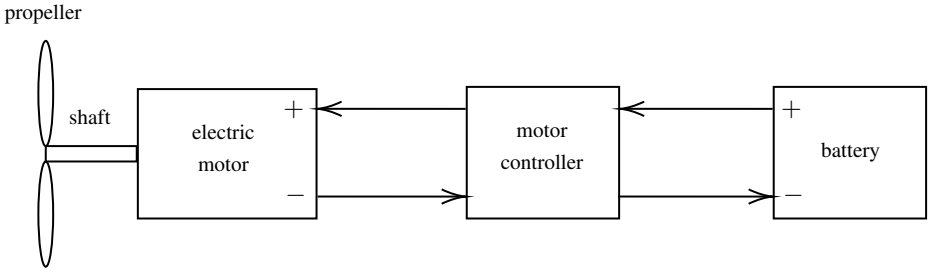

Figure 2. Simplified propulsion system block diagram.

Although the brushless DC motor works with current pulses, its performance can be analyzed as if the motor worked with direct current, in the same way as a brushed DC motor. In this case, the RMS (root mean square) current, voltage and power values are employed. This is a common approach, e.g. (Gur and Rosen, 2009), and manufacturers usually provide brushless motors data in RMS values, e.g. (EMRAX, 2020).

The electric motor is represented by an equivalent lumped circuit model, depicted in Fig. 3, where R_m is the motor internal resistance; i is the electric current flowing through the circuit; U_m is the motor counter-electromotive force; Q_m is the motor torque; and Ω is the motor rotational (angular) speed, in radians per second. No gearbox is considered in the present work, so both motor and propeller have equal rotational speeds.

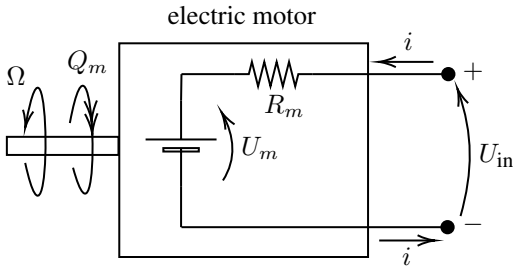

Figure 3. Electric motor circuit diagram.

The motor model is represented by Eqs. (10) and (11) (Gur and Rosen, 2009). The torque is assumed to be proportional to the difference between the electric current i and the motor no-load current i_0. The counter-electromotive force is assumed to be proportional to the rotational speed. Both equations make use of constants K_Q and K_V, which are motor properties.

$$Q_m = (i - i_0)/K_Q \tag{10}$$

$$U_m = \Omega/K_V \tag{11}$$

For a steady state analysis, the motor controller is modeled as a constant resistance R_c, and is assumed to control the voltage applied to the circuit, U_c, such that $0 \leq U_c \leq U_0$. All resistances are summarized into one lumped element R, which represents the total circuit resistance, as shown in Eq. (12):

$$R = R_m + R_c + R_{\text{bat}} \tag{12}$$

Applying Kirchhoff's voltage law to the circuit diagram in Fig. 2, with the total resistance R, results in:

$$R \cdot i = U_c - U_m \tag{13}$$

Substituting the relation presented in Eq. (11) into Eq. (13) and rearranging the terms yields the electric current as a function of the applied voltage U_c and the rotational speed Ω:

$$i = \left(U_c - \frac{\Omega}{K_V} \right) \frac{1}{R} \tag{14}$$

Substituting the result of Eq. (14) into Eq. (10) and rearranging the terms yields Q_m as a function of U_c and Ω:

$$Q_m = \left(U_c - \frac{\Omega}{K_V} \right) \frac{1}{RK_Q} - \frac{i_0}{K_Q} \tag{15}$$

Equation (15) shows that the motor torque Q_m is controlled by adjusting the input voltage U_c, which can be set to an arbitrary value within the voltage range. The rotational speed Ω is achieved when the motor torque equals the propeller torque, this value being influenced by the air density ρ and the aircraft velocity V.

2.5 Example aircraft

An aircraft model based on existing electric motor glider will be used to illustrate the method explained in this article. The relevant aircraft geometric and aerodynamic parameters are shown in Table 1.

Table 1. Example aircraft geometric and aerodynamic parameters.

Parameter	Value	Unit
Wing span (b)	15	m
Wing reference area (S)	12.5	m^2
Max. take-off weight (MTOW)	430	kgf
Zero-lift drag coefficient (C_{D_0})	0.01	–
Lift-dependent drag constant (k)	0.02	–

The aircraft is assumed to be equipped with a fixed pitch, two-blade propeller. The characteristic curves of thrust coefficient C_T and torque coefficient C_Q versus advance ratio J are shown in Fig. 4.

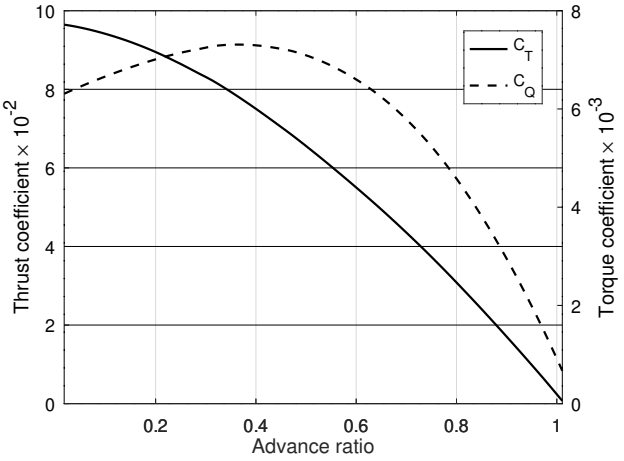

Figure 4. Thrust and torque coefficients versus advance ratio curves for the propeller.

The electric motor and battery data are shown in Table 2.

Table 2. Electric motor and battery data.

Parameter	Value	Unit
Motor internal resistance (R_m)	0.856	ohm
Torque constant (K_Q)	1.333	$\mathrm{A/N \cdot m}$
Speed constant (K_V)	12.732	rpm/V
No-load current (i_0)	220	mA
Battery open-circuit voltage (U_0)	280	V
Battery internal resistance (R_{bat})	0.100	ohm

3. PERFORMANCE ANALYSIS

3.1 Climb velocity and air density

From Eqs. (2) and (3), the velocity can be written as a function of the lift coefficient and the air density, as shown in Eq. (16).

$$V = \sqrt{\frac{2W}{\rho S C_L}} \tag{16}$$

According to the Standard Atmosphere model (NASA/NOAA/USAF, 1976), the air density ρ can be written as a function of the altitude h, as shown by Eq. (17).

$$\rho(h) = \rho_0 \left(1 + \frac{L_{\mathcal{T}}}{\mathcal{T}_0} h\right)^{-\left(1+\frac{gM}{RL_{\mathcal{T}}}\right)} \tag{17}$$

where ρ_0 and $\mathcal{T}_0$ are the air density and temperature at mean sea level, respectively; $L_{\mathcal{T}}$ is the temperature lapse rate; g is the gravitational acceleration, M is the air molar mass and R is the universal gas constant. Equation (17) shows that the air density decreases as altitude increases. Therefore, according to Eq. (16), if the lift coefficient is kept at a constant value, the aircraft velocity must increase as it climbs through the atmosphere. Equation (17) is valid for the troposphere only, that is, for altitudes lower than 11 km. For the tropopause and stratosphere, proper formulas for air temperature and density can be found in (NASA/NOAA/USAF, 1976).

3.2 Maximum propeller rotation attainable

The rotational equilibrium is achieved when the torque load applied by propeller equals the motor torque. For a given altitude h, this condition is expressed in Eq. (18):

$$Q_m(U_c, \Omega) = Q_{\text{pr}}(V, \Omega) \tag{18}$$

It is necessary to choose a velocity for the climb phase. For an electric airplane with a drag polar like the one expressed in Eq. (5), the climb can be performed with the lift coefficient C_L^* shown in Eq. (19) (Barufaldi *et al.*, 2019).

$$C_L^* = \sqrt{\frac{3C_{D_0}}{k}} \tag{19}$$

For the case of a parabolic drag polar, C_L^* is the lift coefficient for minimum required power (Anderson, 1999). Since the altitude is given, the air density is determined with Eq. (17). Therefore, the velocity value associated with C_L^* is given in Eq. (20).

$$V^* = \sqrt{\frac{2W}{\rho S}\sqrt{\frac{k}{3C_{D_0}}}} \tag{20}$$

At the flight condition defined by h and V^*, the maximum propeller rotation is achieved in a full throttle condition, i.e., $U_c = U_0$. Substituting the expressions in Eqs. (7) and (15) in Eq. (18) and rearranging the terms yields an equation in Ω:

$$\left(U_0 - \frac{\Omega}{K_V}\right)\frac{1}{RK_Q} - \frac{i_0}{K_Q} - \rho\, n^2 d^5\, C_Q(J) = 0 \tag{21}$$

Equation (21) can be solved numerically with a non linear solver, yielding the maximum possible rotation Ω_{max}. The rotation frequency n is proportional to Ω; the torque coefficient C_Q is numerically extracted from the propeller chart by interpolation – the advance ratio J is a function of V^* and Ω from Eq. (8). The process is repeated for a wide range of altitude values.

3.3 Rate of climb and ceilings

The vertical component of V is the rate of climb $\dot{h}$. Therefore, rearranging the terms in Eq. (1), and multiplying both sides by V yields:

$$\dot{h} = V \sin\gamma = \frac{V(T - D)}{W} \tag{22}$$

At the flight condition defined by h and V^*, the maximum rate of climb $\dot{h}_{\text{max}}$ is obtained when T is maximum, since D is already defined. From Eq. (6), the maximum thrust value is attained when the propeller reaches the maximum possible rotation Ω_{max}. For each value of h for which the maximum rotation was calculated (as in Sec. 3.2), the corresponding value of $\dot{h}_{\text{max}}$ is computed, until it reaches zero. The rate of climb range is thus obtained, i.e., the altitude range in which a positive rate of climb can be sustained by the aircraft flying at V^*.

The service and absolute ceilings can be numerically computed from Eq. (22) with a non linear solver. Since C_L^* is given, V^* is a function of ρ only and, therefore, a function of h only, via Eq. (17). Since the full throttle condition is imposed, there is only one possible value for the propeller rotation at the flight condition (h, V^*): Ω_{max} and, therefore, Ω also becomes a function of the altitude – the corresponding maximum rotation can be numerically computed by interpolating the values previously obtained in Sec. 3.2. The absolute ceiling h_{ac} is the altitude at which $\dot{h}_{\text{max}} = 0$, and the service ceiling h_{sc} is the altitude at which $\dot{h}_{\text{max}} = 100$ ft/min (approximately 0.5 m/s).

4. RESULTS AND DISCUSSION

The example aircraft and systems shown in Sec. 2.5 are used to exemplify the method presented in this article. The procedures described in Sec. 3.2 are applied to calculate the maximum propeller rotation as a function of the altitude. Figure 5 shows the curve of Ω_{max}, in rpm, versus altitude, in meters. The aircraft is assumed to keep a constant lift coefficient C_L^*, which results in the velocity V^*, calculated with Eq. (20).

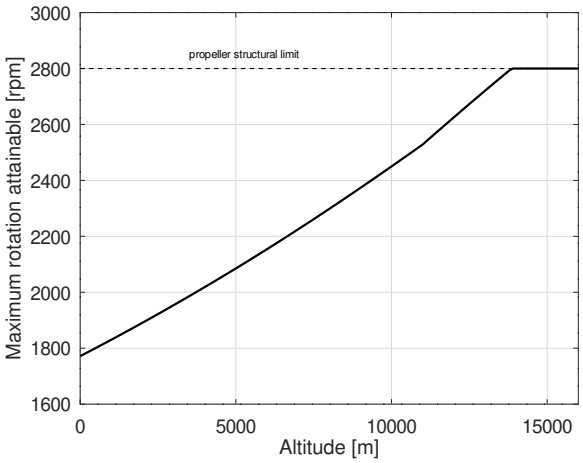

Figure 5. Maximum propeller rotation speed attained as a function of altitude, for $V = V^*$.

Since the air density decreases with increasing altitude, the aerodynamic torque on the propeller also decreases. Therefore, the maximum rotation attained at the full throttle condition increases with altitude. However, the propeller rotation is limited to a "never-exceed" value, due to structural reasons – for this particular propeller, the rotation is limited to 2800 rpm according to the manufacturer.

With the curve in Fig. 5, the procedures described in Sec. 3.3 are employed. Figure 6 shows the maximum rate of climb possible versus altitude. Although there is an increase in the maximum propeller rotation with altitude, it does not offset the decrease in air density, and so the maximum rate of climb also decreases. The rate of decrease however is significantly lower than that of propulsion system based on an internal combustion engine, hence the service and absolute ceilings are significantly higher. For this particular aircraft, flying at its maximum take-off weight (430 kg), the service ceiling is 14557 m ($\approx$ 47760 ft), and the absolute ceiling is 15434 m ($\approx$ 50636 ft).

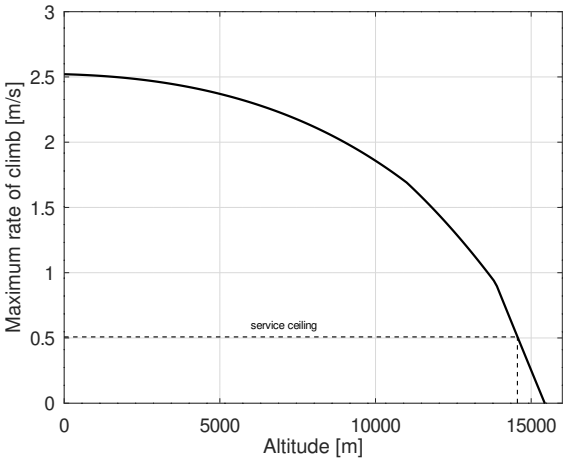

Figure 6. Maximum rate of climb as a function of altitude.

Figure 7 shows the available and required power curves versus altitude. The required power curve shows the necessary power values to fly at given altitude and velocity, i.e., the necessary power to overcome drag. The available power curve shows how much useful power is made available by the propulsion system, in the form of a thrust T at a given velocity. When the required power becomes equal or greater than the available power, the aircraft can no longer climb.

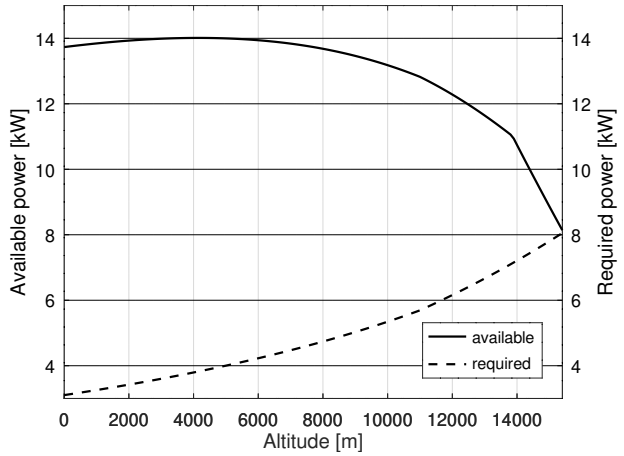

Figure 7. Available power from the propulsion system, and required power to fly, as a function of altitude, for $V = V^*$.

5. CONCLUSIONS

This work has presented a method based on a combination of analytical and numerical procedures for computing the service and absolute ceilings for a battery-powered electric airplane. An example aircraft model based on an existing electric motor glider was presented in parametric form, together with its propulsion system. The maximum propeller rotation $\Omega_{\max}$ was calculated for each altitude, at the velocity associated with the lift coefficient for minimum required power to fly ($C_L^* = \sqrt{3C_{D_0}/k}$). The maximum rotation curve shows that $\Omega_{\max}$ increases with altitude due to the decreasing air density causing the reduction of the aerodynamic torque on the propeller. This phenomenon happens even for a constant voltage supplied by the motor controller (U_c), as show in the article. Therefore, the power available decreases at a significantly lower rate than it would for a propulsion system based on an internal combustion engine. Since the electric motor does not ingest air, its capacity to supply power does not decrease with altitude, and the only factor that causes the reduction of the available power is the reduction in air density – an aerodynamic effect on the propeller, not on the motor. The service and absolute ceilings calculated for the small example motor glider are 14557 m ($\approx$ 47760 ft) and 15434 m ($\approx$ 50636 ft), respectively. These results show that electric aircraft are capable of reaching altitudes significantly higher than those reached by aircraft equipped with an internal combustion engine.

6. ACKNOWLEDGEMENTS

This study was financed in part by the Coordenação de Aperfeiçoamento de Pessoal de Nível Superior – Brasil (CAPES) – Finance Code 001, under the research grant number 88882.180826/2018-01.

7. REFERENCES

Airbus Group, 2017. "Airbus, Rolls-Royce, and Siemens team up for electric future partnership launches E-Fan X hybrid-electric flight demonstrator". URL `http://www.airbus.com/newsroom/press-releases/en/2017/11/airbus--rolls-royce--and-siemens-team-up-for-electric-future-par.html`. Retrieved 9 Jun. 2018.

Anderson, J.D., 1999. *Aircraft Performance and Design*. McGraw-Hill, New York, 1st edition.

Anderson, J.D., 2010. *Fundamentals of Aerodynamics*. McGraw-Hill Education, New York, NY, 5th edition.

Barufaldi, G.N., Morales, M.A.V. and da Silva, R.G.A., 2019. "Energy Optimal Climb Performance of Electric Aircraft". In *AIAA SciTech Forum*. doi:10.2514/6.2019-0830.

Brelje, B.J. and Martins, J.R.R.A., 2019. "Electric, hybrid, and turboelectric fixed-wing aircraft: a review of concepts, models, and design approaches". *Progress in Aerospace Sciences*, Vol. 104, pp. 1–19. doi:10.1016/j.paerosci.2018.06.004.

EMRAX, 2020. "EMRAX 268 motor technical data". EMRAX E-Motors. URL `https://emrax.com/wp-content/uploads/2020/03/emrax_268_technical_data_table_graphs_5.4.pdf`. Retrieved on May 8, 2020.

Gur, O. and Rosen, A., 2009. "Optimizing electric propulsion systems for unmanned aerial vehicles". *Journal of Aircraft*, Vol. 46, No. 4, pp. 1340–1353. doi:10.2514/1.41027.

Hepperle, M., 2012. "Electric Flight – Potential and Limitations". In *Proceedings of the NATO Science and Technology Organization Meeting*. Vol. 209.

Lange Aviation, 2003. "The Antares 20E". URL `https://www.https://www.lange-aviation.com/en/produkte/antares-20e/`. Retrieved on May 24, 2020.

Moore, M.D. and Fredericks, B., 2014. "Misconceptions of Electric Propulsion Aircraft and their Emergent Aviation Markets". AIAA Paper 2014-0535.

NASA/NOAA/USAF, 1976. *U.S. Standard Atmosphere*. National Aeronautics and Space Administration, National Oceanic and Atmospheric Administration, United States Air Force.

Raymer, D.P., 2006. *Aircraft Design: A Conceptual Approach*. AIAA Education Series. American Institute of Aeronautics and Astronautics, Reston, VA, 4th edition.

Sachs, G., 2013. "Unique Range Performance Properties of Electric Aircraft". In *AIAA Atmospheric Flight Mechanics Conference*. doi:10.2514/6.2013-5088.

Tremblay, O. and Dessaint, L.A., 2009. "Experimental Validation of a Battery Dynamic Model for EV Applications". *World Electric Vehicle Journal*, Vol. 3, pp. 289–298.

Von Mises, R., 1945. *Theory of Flight*. Dover Publications, New York. Pp. 285-316.

8. RESPONSIBILITY NOTICE

The authors are solely responsible for the printed material included in this paper.